ACS OMEGA

Open Access

http://pubs.acs.org/journal/acsodf

Article

Preparation and Rheological Properties of the PVA/CMC/Gel Composite for Mining

Xiaonan Shi, Baiqian Wu, Xuechao Dong, Qian Zhang,* Wei Lu, and Xiaolin Chen

Cite This: *ACS Omega* 2024, 9, 28253−28267

Read Online

ACCESS | Metrics & More | Article Recommendations

ABSTRACT: A composite gel material with an interpenetrating network structure was formed using the chemical cross-linking method. The viscosity, yield stress, and thixotropy of a poly(vinyl alcohol)/carboxymethyl cellulose/gelatin (PVA/CMC/Gel) composite gel slurry with different ratios were tested using a viscometer, and the interaction between the surface of the gelling agent and the cross-linking agent was analyzed by calculating the frontline orbital energy of a single polymer material molecule. The seepage diffusion characteristics of the composite gel in a goaf were then studied through a numerical simulation. The results indicate that the PVA/CMC/Gel composite gel exhibits shear thinning behavior following the power law model and behaves as a pseudoplastic fluid. The optimal ratio for the composite gel at 30 °C is determined as follows: 30 wt % for the gelling agent (PVA/(Gel + CMC) = 20:10), 4 wt % for the cross-linking agent, 3.09 wt % for the carbide slag, 7.5 wt % for the alcohol amine solution, and 0.5% sodium dodecyl sulfonate + 0.1% alkyl glycoside for the foaming agent. Gel exhibits the lowest energy band gap (0.096 eV), indicating strong reaction activity and strong reaction with the cross-linking agent (sodium tetraborate). PVA has the largest energy band gap (0.238 eV), strong molecular stability, and weak reaction with the cross-linking agent (sodium tetraborate). When the dip angle of the goaf is 4° and the injection time is 40 min, the composite gel tends to diffuse more easily along the dip. The investigation into the rheological properties of the PVA/CMC/Gel composite gel holds significant importance in the design of coal mine pipeline transportation and understanding diffusion flow in goaf.

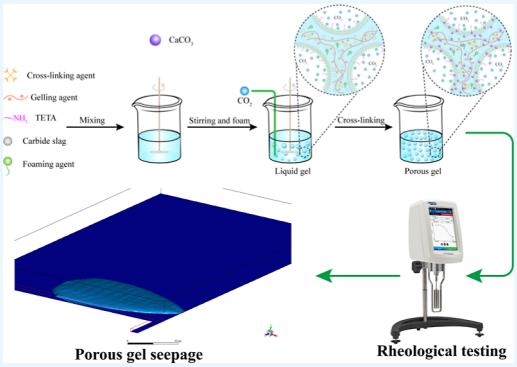

1. INTRODUCTION

Coal plays a crucial role as a nonrenewable energy source in China. In 2022, the country achieved a record high coal production of 4.496 billion tons. However, the threat of coal spontaneous combustion is a significant concern in more than 130 coal mining areas across 25 major coal-producing provinces and regions. By the end of October 2021, out of the 4113 operating coal mines in China, 2392 mines (accounting for 58.2% of the total) were either prone to spontaneous combustion or had coal seams with a high susceptibility to it. These incidents not only endanger miners' lives but also disrupt the extraction of coal resources and can lead to thermodynamic disasters like gas explosions.[1,2]

One of the primary causes of coal spontaneous combustion is the favorable oxygen supply conditions found in coal. To prevent and control coal spontaneous combustion, it is crucial to block oxygen supply or reduce oxygen concentration.[3] Currently, common methods used to reduce oxygen and extinguish fires include injecting slurry, foam,[4] and inert gas.[5] Among these methods, high-water gel[6−8] can rapidly vaporize and absorb heat when it comes into contact with high-temperature coal, effectively reducing the surface temperature of the coal and encapsulating it to seal air leaks and isolate oxygen. Coal spontaneous combustion often occurs in the deep goaf or inside coal pillars, where external signs are not obvious, making it difficult to identify the ignition source through sensory perception. Additionally, the complex factors affecting colloids, such as different compositions, temperatures, and shear rates, can result in varying viscosities of the gel foam. Therefore, it is not possible to interpret the rheological properties of gel foam solely on the basis of the relationship between gel foam viscosity and mass. Consequently, conducting in-depth research on the rheological properties of colloids and other influencing factors (such as gel foam ratio, temperature, shear rate, etc.) holds great significance for the design of coal mine pipeline transportation, goaf diffusion flow, and achieving both direct and indirect fire extinguishing performance goals.

Currently, research on the diffusion of slurries is primarily focused on theoretical derivation, model experiments, and

Received: February 21, 2024
Revised: June 8, 2024
Accepted: June 12, 2024
Published: June 20, 2024

Table 1. Components and Their Proportions in Carbide Slag

components	CaO	SiO_2	Al_2O_3	Na_2O	MgO	SO_3	Fe_2O_3	other
content (%)	95.963	1.429	0.982	0.646	0.263	0.247	0.210	0.260

Table 2. Proportions of the Composite Gel

sample number	polymer (g)	cross-linker (g)	SDS:APG (wt %)	carbide slag (g)	TETA solution (g)	water
1	5:25	2	0.5:0.1	3.09	7.5	56.81
2	10:20	2	0.5:0.1	3.09	7.5	56.81
3	15:15	2	0.5:0.1	3.09	7.5	56.81
4	20:10	2	0.5:0.1	3.09	7.5	56.81
5	5:25	4	0.5:0.1	3.09	7.5	54.81
6	10:20	4	0.5:0.1	3.09	7.5	54.81
7	15:15	4	0.5:0.1	3.09	7.5	54.81
8	20:10	4	0.5:0.1	3.09	7.5	54.81
9	5:25	6	0.5:0.1	3.09	7.5	52.81
10	10:20	6	0.5:0.1	3.09	7.5	52.81
11	15:15	6	0.5:0.1	3.09	7.5	52.81
12	20:10	6	0.5:0.1	3.09	7.5	52.81

numerical simulations conducted both domestically and internationally. In terms of grouting theory, researchers have developed a series of theoretical formulas based on fluid mechanics, seepage mechanics, and solid mechanics, which have been optimized. For instance, Liu et al.[9] considered the time-varying characteristics of slurry viscosity and derived the diffusion equation for crack grouting. Niu et al.[10] designed a three-dimensional simulation grouting test system and improved the theory of fissure grouting in filling zones. Feng et al.[11] established a theoretical model for the density of slurry in porous media under the combined influence of convection, diffusion, and permeation based on the law of mass conservation and the linear permeation law using Laplace transform. Regarding model experiments and numerical simulations, Li[12] proposed the sequential diffusion solidification method to simulate dynamic grouting. Zhang et al.[13] analyzed the variation of rock mass elastic modulus after grouting under different viscosities using numerical simulation. Liang et al.[14] derived a radial diffusion model for polymer single crack grouting based on the diffusion mechanism of foam polymer slurry in rock fractures. However, existing studies face challenges in simplifying slurry as a Newtonian fluid to calculate its diffusion distance due to the concealment of model test sites, the randomness of materials, and the complexity of the environment.[15,16] Therefore, it is necessary to simulate the seepage and diffusion of colloidal materials in coal mines to provide a theoretical basis for their engineering applications in loose coal bodies.

In this study, a composite gel material with an interpenetrating network structure was formed using the chemical cross-linking method. Natural high molecular weight materials and industrial solid waste were utilized, and a cross-linking agent [poly(vinyl alcohol), carboxymethyl cellulose, gelatin, and sodium tetraborate] was employed to undergo chemical cross-linking reactions, resulting in the formation of the first network structure. Additionally, the calcium carbide slag clarification solution underwent chelation reactions to form the second network structure. Through the action of a surfactant, the first and second networks intersected, leading to the formation of a composite gel material with an interpenetrating network structure. The relationship between the apparent viscosity of the gel foam and the shear rate was investigated using a viscometer for various ratios of the gelling agent to the cross-linking agent. This analysis determined the mathematical model of shear stress and shear rate as well as the rheological properties of the gel foam. Furthermore, Fluent software was employed to numerically simulate the accumulation and diffusion of the composite gel material in goaf, allowing for the acquisition of parameters such as accumulation height and diffusion width. These findings provide valuable insights for the application of composite gel materials in coal mine sites, thereby contributing to the advancement of mine fire prevention technology and ensuring safe production in mines.

2. MATERIALS AND METHODS

2.1. Materials. The required raw materials for the experiment are as follows: gelling agent (polysaccharide polymer material), cross-linking agent (borax), foaming agent (SDS and APG), alcohol amine solution, carbide slag, and CO_2 gas. Quantitative analysis of various components in the calcined calcium carbide slag was conducted using an X-ray fluorescence spectrometer (as shown in Table 1), and the results showed that the proportion of calcium oxide in the calcined calcium carbide slag was close to 96%.

2.2. Preparation of the PVA/CMC/Gel Composite. The flask should be prepared by adding the appropriate amount of gelatinizer, carbide slag, TETA, foaming agent, and cross-linking agent in sequence. The mixture should be stirred evenly using a mechanical stirrer. At the same time, a certain flow rate and concentration of CO_2 should be introduced. Once the composite gel is cross-linked and stabilized, the gas flow should be stopped and the stirrer turned off.

2.3. Characterization Test Methods. *2.3.1. Physicochemical Analysis.* The components of the composite gel were analyzed using a Nicolet iS50 Fourier Transform Infrared Spectrometer (Thermo Fisher Scientific, USA). The chemical composition and content of the samples were determined by using a Bruker X-ray Fluorescence Spectrometer.

2.3.2. Rheological Performance Testing. To begin the experiment, 100 mL of the test sample that has been prepared under different conditions (such as using different gelatinizers, cross-linking agent ratios, and pH values) was measured and placed in a plastic cup. Then, the protective frame of the NDJ-

https://doi.org/10.1021/acsomega.4c01502
ACS Omega 2024, 9, 28253−28267

5S viscometer was inserted into the lower end of the instrument. The no. 3 rotor was attached to the instrument head (when the rotor speed is 60, 30, 12, and 6 rpm, the corresponding fluid viscosity ranges are 2000, 4000, 10 000, and 20 000 mPa·s, respectively). The no. 3 rotor was slowly lowered into the test sample using the up and down switch until the groove on the rotor rod is at the same level as the measured composite gel. The rotor selection button was pressed, and the numerical value displayed on the viscometer screen was noted, which indicates the apparent viscosity of the test sample.

2.3.3. Thixotropic Performance Test. The sample will transform into a thixotropic fluid with changes in shear rate (stress) and time.[17] When conducting thixotropy testing, the shear rate is increased from 4.239 to 42.390 s^{-1} in sequence. The corresponding apparent viscosity values are recorded on the viscometer display screen to obtain the relationship curve between the apparent viscosity and shear rate. Then, the maximum shear rate is sequentially decreased to 4.239 s^{-1}, and the corresponding apparent viscosity values on the display screen are repeatedly recorded to obtain another curve of apparent viscosity and shear rate. The collected data are imported into Origin for linear fitting. By observation of whether the two curves overlap, it can be determined whether the sample being tested exhibits thixotropy. The specific ratio of each group of samples is shown in Table 2.

2.3.4. Computational Details. In this study, the geometric structure of the composite gel [poly(vinyl alcohol)/carboxymethyl cellulose/gelatin (PVA/CMC/Gel)] was optimized using density functional theory and B3LYP. The results were obtained using DMol3, version 2020. When the DMol3 calculation method is used to process target molecules, several calculation parameters need to be selected and adjusted according to different calculation tasks, molecular structure characteristics, and calculation purposes.

2.3.5. Study on Seepage Diffusion Characteristics of Composite Gel in Goaf. This study presents a goaf model based on a specific working face in a coal mine located in the Shaanxi Province. The dimensions of the goaf model are as follows: 360 m in length, 220 m wide, and 20 m high. The working face has a width of 8 m, while the roadway width is 3.5 m. Both the working face and roadway have widths of 3 m. The geometric model of the goaf can be visualized in Figure 1.

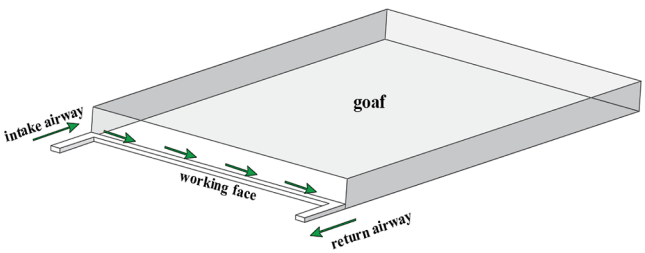

Figure 1. Schematic diagram of the goaf model structure.

The composite gel is used for grouting along the embedded pipes at the bottom of the air return roadway side of the goaf. The distance between the grouting pipe orifice and the working face is 35 m, and the pipe diameter is 0.108 m. The inclination angles of the goaf along the dip are set at 2, 4, 6, and 10°, respectively. The grouting inlet velocities are set at 4, 7, and 10 m^3/h. The main parameters and boundary conditions for establishing the model are listed in Table 3.

Table 3. Main Parameters of the Goaf Model

serial number	paraments	parameter value
1	size of goaf	360 m long, 220 m wide, and 20 m high
2	working face size	220 m long, 8 m wide, and 3 m high
3	tunnel size	width 3.5 m, height 3 m
4	dip angle of goaf	set 2, 4, 6, and 10°, respectively, with inclination angles
5	inlet velocity	set to 4, 7, and 10 m^3/h, respectively
6	viscosity of composite gel	$\eta = -55\gamma + 76\,423/\gamma + 5417$

3. RESULTS AND DISCUSSION

3.1. Rheological Properties of the Composite Gel under Different Ratios. At a room temperature of 20 °C, the composite gel samples were prepared by changing the ratio of PVA and Gel + CMC in the gelatinizer and the amount of cross-linking agent added. The fixed foaming agent (0.5% SDS:0.1% APG) mass concentration, calcium carbide slag mass (3.09 g), alcohol amine solution mass (7.5 g), and amount of gelatinizer added (30 g) remained constant. The CO_2 gas flow rate was kept the same. The apparent viscosity (η) of the composite gel with different ratios was determined by measuring the shear rate (γ).

The relationship between the apparent viscosity of the composite gel and the shear rate is shown in Figure 2. It can be observed that the apparent viscosity of the composite gel exhibits a linear relationship with the shear rate regardless of the different ratios. When the fixed cross-linking agent amount was 2 and 4 g, the apparent viscosity of the composite gel increased as the proportion of PVA in the polymer increased. Additionally, the apparent viscosity of the composite gel decreased with an increasing shear rate, indicating a typical shear thinning non-Newtonian fluid behavior. Furthermore, Figure 2a,b demonstrates that the apparent viscosity of the composite gel increased with an increase in the amount of cross-linking agent while maintaining a constant proportion of the fixed polymer. However, when the amount of cross-linking agent was further increased to 6 g, the apparent viscosity of the composite gel did not increase with an increase in the proportion of PVA in the polymer. Interestingly, when the ratio of PVA to (Gel + CMC) was 20:10, the apparent viscosity of the composite gel decreased.

When a low amount of PVA is added to the cross-linking agent or polymer, the active sites of the borate ions in the cross-linking agent decrease, reducing the formation of an effective spatial network structure. This results in a straightened orientation of the molecular structure chain, leading to a lower flow resistance and a lower apparent viscosity. However, as the amount of PVA and cross-linking agent increases, more effective cross-linking occurs between the gelling agent and cross-linking agent. The linear molecular chains in the system become intertwined, making it difficult for the flow caused by relative molecular motion. This increases the difficulty of shear in the system. While increasing the concentration of gelling or cross-linking agents can increase the viscosity of the system and shorten the gelling time, it can also reduce flowability, which may cause pipe blockage accidents during application and fail to meet on-site requirements.

In order to investigate the impact of various gelling agents and cross-linking agents on the apparent viscosity of a composite gel, the rheological properties of the gel were

https://doi.org/10.1021/acsomega.4c01502
ACS Omega 2024, 9, 28253−28267

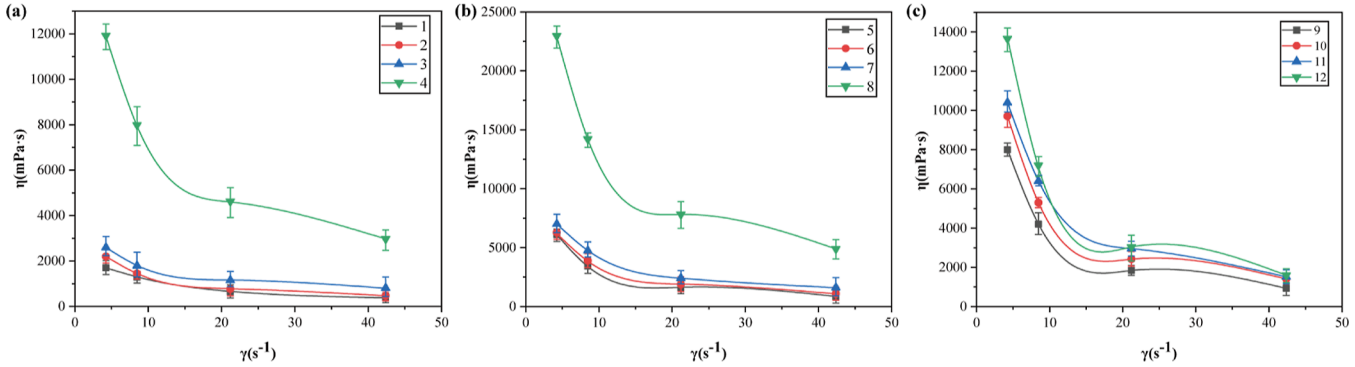

Figure 2. Rheological curve of the composite gel at different ratios: (a) samples 1−4; (b) samples 5−8; and (c) samples 9−12.

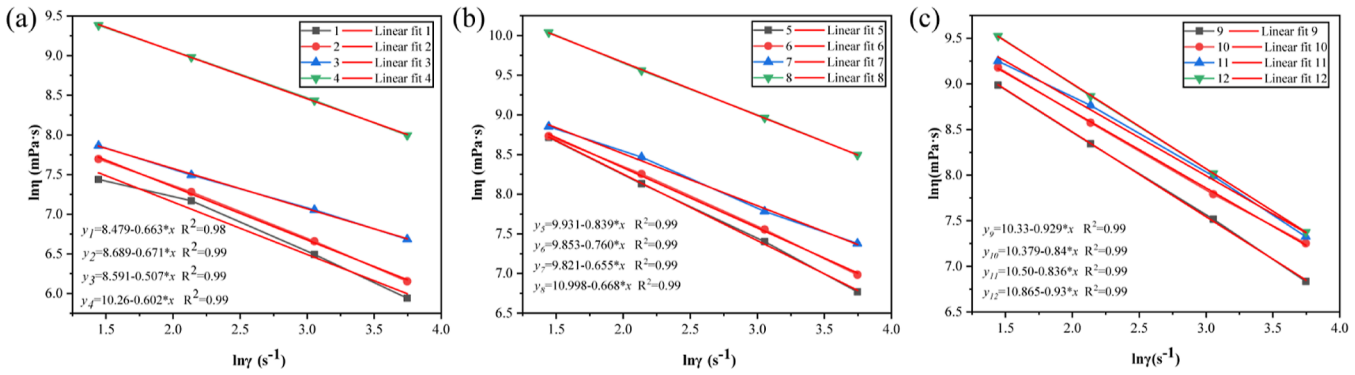

Figure 3. Relationship between ln η and ln γ of the composite gel under different dosage of gels and cross-linkers: (a) samples 1−4; (b) samples 5−8; and (c) samples 9−12.

Table 4. Viscosity Index and Viscosity Coefficient of the Composite Gel when the Cross-Linking Agent is 2g

hierarchy	power law index (n)	viscosity coefficient (k)	R^2
1	0.337	4812.63	0.98
2	0.666	5337.24	0.99
3	0.493	5782.99	0.99
4	0.398	28 566.78	0.99

Table 5. Viscosity Index and Viscosity Coefficient of the Composite Gel when the Cross-Linking Agent is 4g

hierarchy	power law index (n)	viscosity coefficient (k)	R^2
5	0.161	20 557	0.99
6	0.24	21 015	0.99
7	0.345	24 416	0.99
8	0.332	59 754	0.99

Table 6. Viscosity Index and Viscosity Coefficient of the Composite Gel when the Cross-Linking Agent is 6g

hierarchy	power law index (n)	viscosity coefficient (k)	R^2
9	0.071	30 638	0.99
10	0.16	32 176	0.99
11	0.164	36 315	0.99
12	0.07	52 312	0.99

analyzed using the Ostwald model logarithmic form (Formula 1).[18]

$$\ln \eta = \ln k + (n - 1)\ln \gamma \quad (1)$$

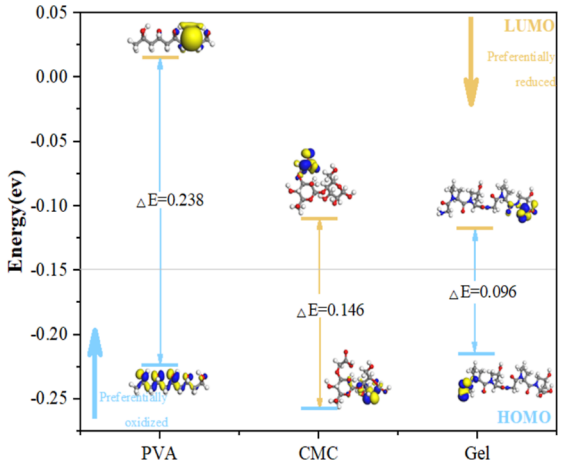

Figure 4. Frontline orbital energy map.

In the equation, η represents the apparent viscosity in m·Pa·s, k represents the viscosity coefficient, γ represents the shear rate in s^{-1}, and n represents the power law index. The power law index measures non-Newtonian behavior, with a smaller value indicating a more curved curve and stronger non-Newtonian behavior. The viscosity coefficient (k) is a measure of viscosity with higher values corresponding to higher viscosity.

A graph should be plotted with ln η as the y-axis and ln γ as the x-axis, as shown in Figure 3. Linear regression should be performed on the experimental data using the "power law model" to obtain the viscosity coefficient k and power law index n from the slope and intercept of the fitted line,

https://doi.org/10.1021/acsomega.4c01502
ACS Omega 2024, 9, 28253−28267

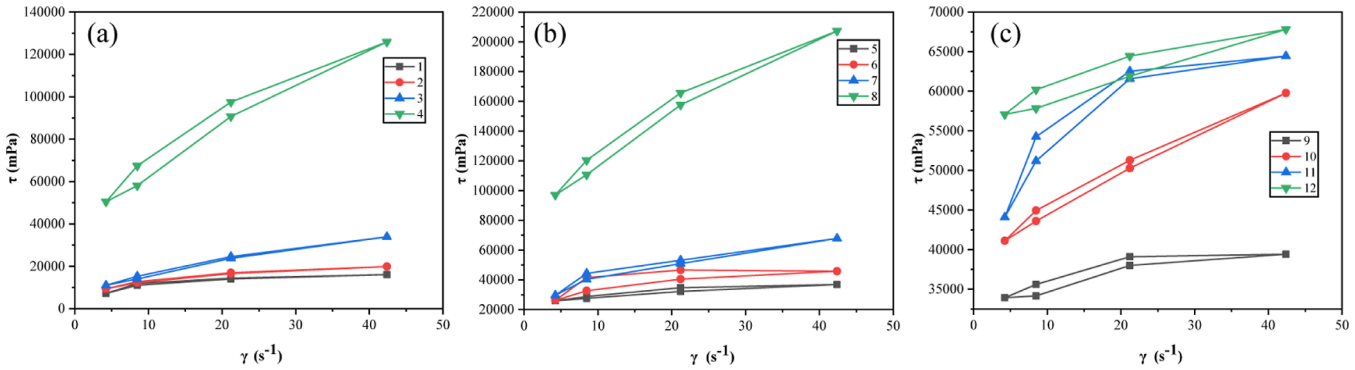

Figure 5. Thixotropic response of composite gel with different ratios: (a) samples 1−4; (b) samples 5−8; and (c) samples 9−12.

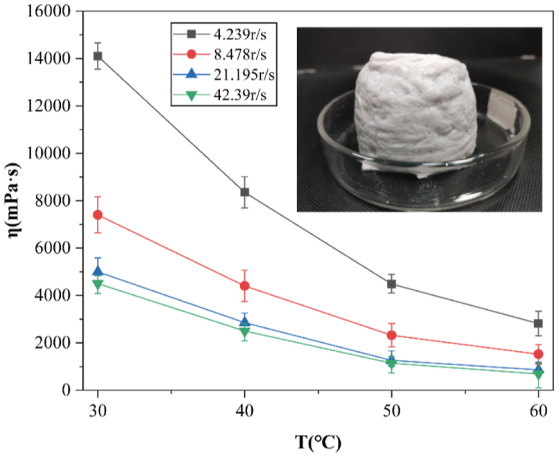

Figure 6. Effect of temperature on apparent viscosity of the composite gel at different shear rates.

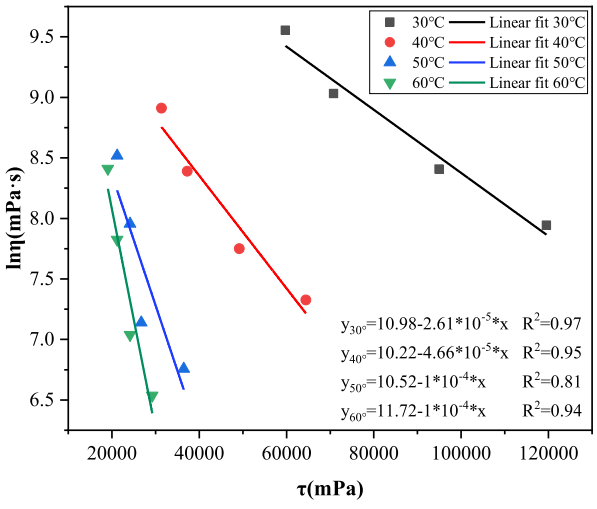

Figure 7. Plot the graph of ln η against τ for the composite gel at different temperatures.

Table 7. Effects of Different Temperatures on the Viscosity of Porous Gel Samples

T/°C	ln η_0	R^2
30	10.98	0.97
40	10.22	0.95
50	10.52	0.81
60	10.72	0.94

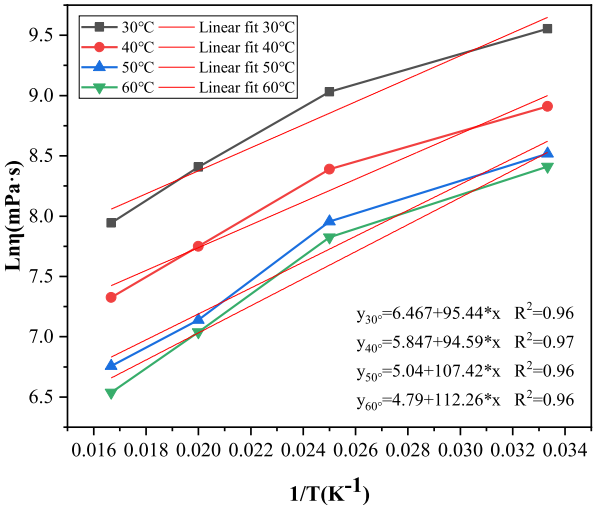

Figure 8. Plot of the graph of ln η against T^{-1} for the composite gel.

Table 8. Parameters of the Composite Gel at Different Temperatures

T/°C	A	E_a	R^2
30	643.55	240 426	0.96
40	346.19	246 149	0.97
50	154.47	287 340	0.96
60	120.30	310 798	0.96

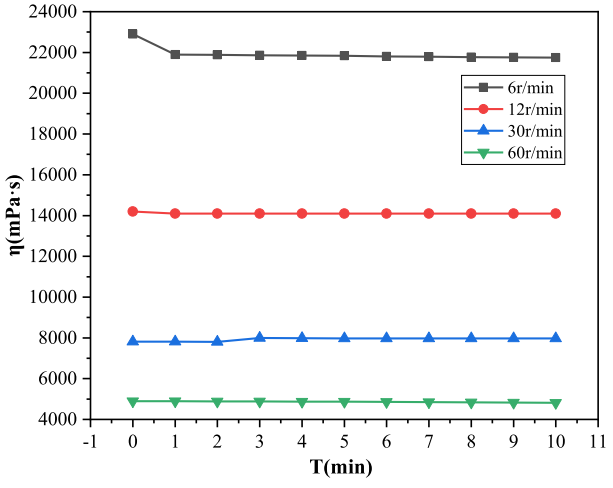

Figure 9. Shear stability of the composite gel.

https://doi.org/10.1021/acsomega.4c01502
ACS Omega 2024, 9, 28253−28267

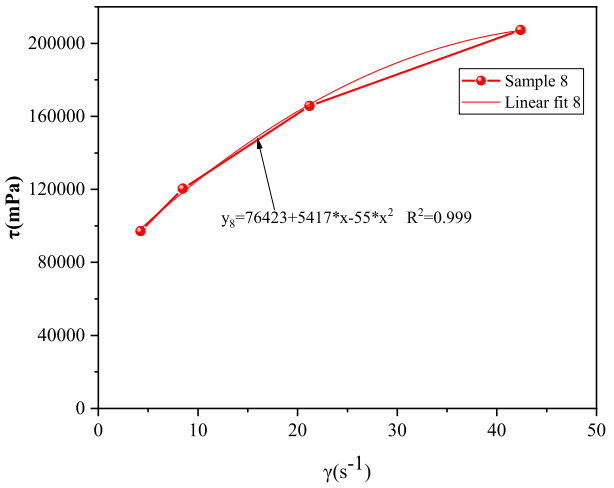

Figure 10. Curve of shear stress and shear rate of the composite gel.

respectively. These values are listed in Table 4. Non-Newtonian fluids can be classified into two types: pseudoplastic fluids and dilatant fluids. Pseudoplastic fluids are characterized by a decrease in viscosity with increasing shear rate under stable shear flow, with a power law index (n) less than 1. Dilatant fluids, on the other hand, are characterized by an increase in viscosity with increasing shear rate under stable shear flow, with a power law index (n) greater than 1.

From Figure 3, it can be observed that the amount of fixed cross-linking agent (2, 4, or 6 g) is determined by ln η for ln γ. The rheological curve of the composite gel system exhibits a linear function relationship with a similarity coefficient (R^2) greater than 0.98. This suggests that there is a logarithmic relationship between the apparent viscosity of the composite gel and the shear rate, following the power law model. The power law exponent (n) values are all less than 1, indicating that the system behaves as a pseudoplastic fluid. The apparent viscosity of the composite gel increases as the proportion of PVA in the polymer increases, indicating that the viscosity of the composite gel also increases with a higher proportion of PVA. Therefore, the composite gel system exhibits the characteristics of a non-Newtonian fluid. When the amount of cross-linking agent is 2 g as shown in Table 4, the power law index of the composite gel follows the order: n1 < n4 < n3 < n2 < 1. Similarly, when the amount of the cross-linking agent is 4 g as shown in Table 5, the power law index follows the order n5 < n6 < n8 < n7 < 1. When the amount of the cross-linking agent is 6 g as shown in Table 6, the power law index of the composite gel follows the order n12 < n9 < n10 < n11 < 1. These results indicate that the non-Newtonian properties of the composite gel vary under different ratios of polymer and cross-linking agent. In particular, when PVA/(Gel + CMC) = 5:25 and the amount of cross-linking agent is 2 g, the viscosity coefficient of the composite gel is 4812.63, which is the smallest value observed in this system. The limited amount of the cross-linking agent and polymer results in a small effective content. The borate ion in the cross-linking agent reacts with the hydroxyl group in the system, but there are only a few active sites available for this reaction. As a result, an effective spatial network structure cannot be formed. The molecular structure chain remains in a straight orientation, resulting in low flow resistance and a nongelatinous appearance. However, when the proportion of PVA in the gelling agent and the amount of cross-linking agent increase, more sites become involved in the cross-linking reaction. This leads to enhanced cross-linking between the gelling agent and the cross-linking agent. Consequently, the linear molecular chains in the system become entangled, making molecular movement and flow more difficult. As a result, the system exhibits increased shear difficulty, and the apparent viscosity of the composite gel increases. In the specific case of PVA/Gel + CMC = 20:10 and 4 g of cross-linking agent, the viscosity coefficient of the composite gel is 59 754, which is the highest in this system, indicating the superior cross-linking property of the composite gel in this particular system.

In order to analyze the interaction between the gelling agent and the cross-linking agent surface from an energy perspective, we calculated the frontier orbital energy of a single polymer material molecule as shown in Figure 4. This calculation was done using the Dmol3 module[19−21] to determine the highest occupied molecular orbital (HOMO) and lowest unoccupied molecular orbital (LUMO) energies. The HOMO value indicates the ease of losing electrons, while the LUMO value indicates the ease of receiving electrons. The energy difference between the two, known as the "energy band gap", is an important indicator of reaction stability. A smaller energy band gap suggests a higher reaction activity and excitability of the molecule. Gelatin (Gel) has the lowest energy band gap (0.096 eV), indicating strong reaction activity and a strong reaction with the cross-linking agent (sodium tetraborate). On the other hand, PVA has the largest energy band gap (0.238 eV), suggesting strong molecular stability and a weak reaction with the cross-linking agent (sodium tetraborate).

3.2. Thixotropic Properties of the Composite Gel under Different Ratios. Based on the rheological property research of the composite gel, further investigation was conducted on the thixotropy of the composite gel. The thixotropy of the composite gel at different ratios is illustrated in Figure 5.

Thixotropic fluids are characterized by their time-dependent response to external stress. When a thixotropic fluid flows, a network structure is formed between particles, leading to structural damage. However, when the flow ceases, the structure of the fluid recovers. Both the damage and recovery processes require a certain amount of time, resulting in a significant time dependence in the flow properties of the system. Figure 5 illustrates the thixotropy curve of a composite gel under different polymer proportions and cross-linking agent parameters. In Figure 5a, it can be observed that the shear stress curves of the composite gel system during the rise and fall stages of the shear rate approximately coincide when the cross-linking agent is added in an amount of 2 g, and the PVA/(Gel + CMC) ratio in the gelling agent is 5:25, 10:20, and 15:15. This suggests that the thixotropy of the composite gel is not significant when the proportion of PVA in the gelling agent is low. However, when the ratio of PVA/(Gel + CMC) is 20:10, the rheological curve of the composite gel exhibits a "hysteresis loop" after rising and falling. By performing integral calculation, it is determined that the area of the hysteresis loop is 194 066.51, indicating the presence of thixotropy in the composite gel system at this ratio. Furthermore, increasing the amount of cross-linking agent to 4 g results in noncoinciding shear stress curves of the composite gel system during the increase and decrease of the shear rate, and the rheological curves of the composite gel exhibit a "hysteresis loop" after rising and falling. The area of the hysteresis loop is calculated by integration as follows: S5 = 53 547.98, S6 = 179 691.21, S7

https://doi.org/10.1021/acsomega.4c01502
ACS Omega 2024, 9, 28253−28267

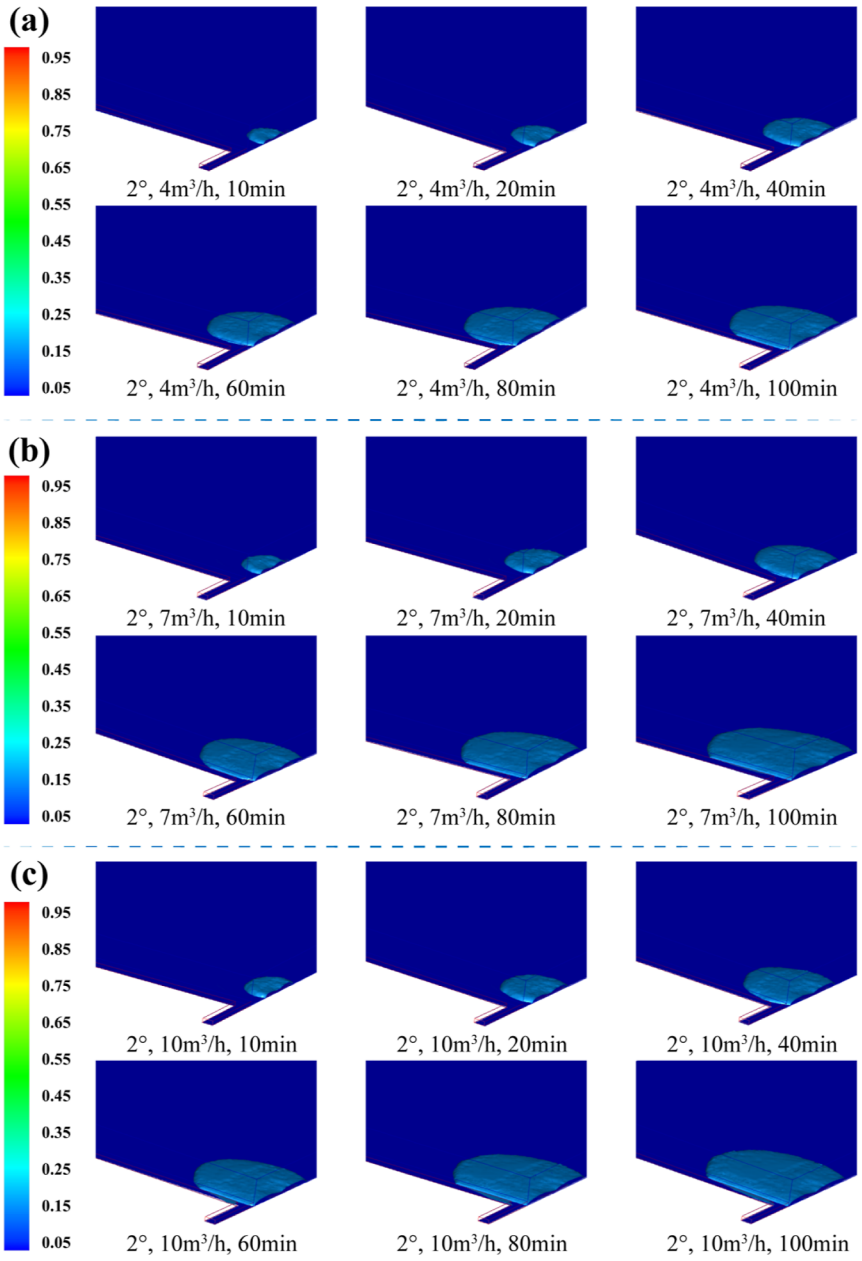

Figure 11. Seepage diffusion state of the composite gel when the dip angle of goaf is 2°: (a) 4; (b)7; and (c)10 m^3/h.

= 73 885.89, and S8 = 218 863.89. The hysteresis loop area follows the order S5 < S7 < S6 < S8, indicating that the thixotropy of the composite gel is not significant when the proportion of PVA in the gelling agent is low. However, as the proportion of PVA increases in the gelling agent, the thixotropy of the composite gel becomes more pronounced. When the dosage of the cross-linking agent is 6 g (as shown in Figure 5c), the integral calculation reveals that the area of the hysteresis loop is S9 = 31 034.57, S10 = 28 291.93, S11 = 41 818.41, and S12 = 63 083.95. The order of the hysteresis loop area is sorted as follows: S10 < S9 < S11 < S12. This indicates that with the addition of more cross-linking agents, the composite gel exhibits significant thixotropy, while the gelling agent has minimal impact on the thixotropy of the composite gel.

At a specific shear rate, thixotropic fluids exhibit a decrease in apparent viscosity with an increase in shear rate and an increase in apparent viscosity with a decrease in shear rate after reaching a certain point. This behavior can be attributed to the process of gel formation from a polymer solution, where the viscosity of the system increases and the molecular structure transforms from an irregular chain to a three-dimensional cross-linked network. Under shear stress, the molecular chains align, and the entangled nodes decrease, disrupting the equilibrium three-dimensional network structure and resulting in a decrease in apparent viscosity, thus demonstrating thixotropic properties. Subsequently, when the composite gel transitions to a semigel flowable state due to shear-induced thixotropy, the system's viscosity decreases. Weak bond cross-linking points, such as hydrogen bonds, break in the structure, but the molecular structure remains unchanged. If the solution is left undisturbed for a period of time, then a new composite gel is formed again, leading to an increase in system viscosity without any change in molecular structure. However, the

https://doi.org/10.1021/acsomega.4c01502
ACS Omega 2024, 9, 28253−28267

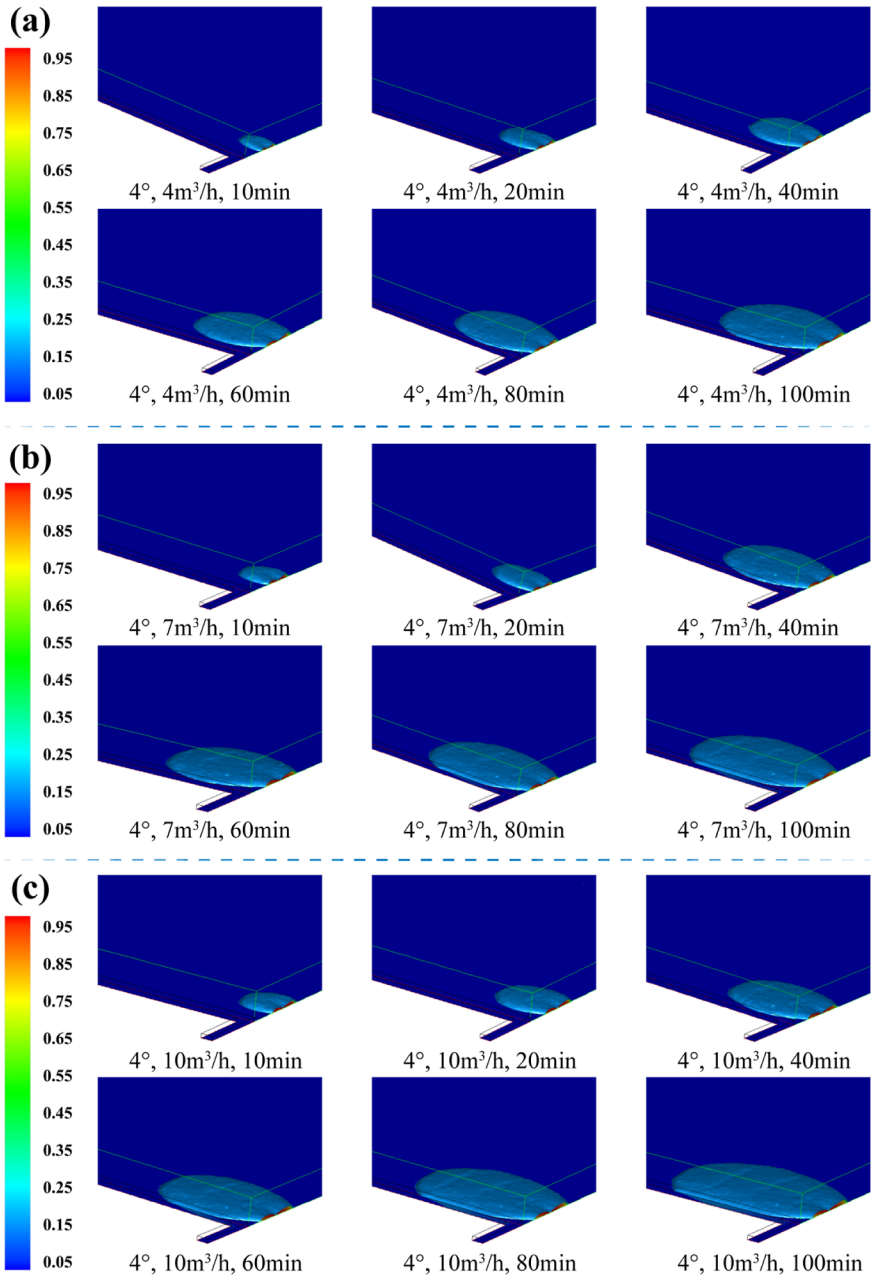

Figure 12. Seepage diffusion state of the composite gel when the dip angle of goaf is 4°: (a) 4; (b) 7; and (c) 10 m^3/h.

reconnected hydrogen bonds cannot fully restore the preshearing state. Moreover, as the proportion of PVA in the polymer increases, the presence of weak bond cross-linking points, such as hydrogen bonds, also increases, gradually enhancing the thixotropic behavior of the system.

After comprehensive consideration, the amount of cross-linking agent added is 4 g, PVA/(Gel + CMC) = 20:10, and other ratios remain unchanged for subsequent testing.

3.3. Rheological Properties of the Composite Gel at Different Temperatures. The mass concentration of the foaming agent (0.5% SDS + 0.1% APG), the mass of carbide slag (3.09 g), the mass of TETA (7.5 g), the addition amount of the gelling agent (30 g), and the CO_2 gas flow remained unchanged, while other conditions remained constant. Gel samples were tested for their apparent viscosity at different temperatures (30, 40, 50, and 60 °C) to determine the impact of temperature variations on their rheological properties. The test results are presented in Figure 6.

The results presented in Figure 6 indicate that the viscosity of the composite gel sample decreases as the shear rate increases at the same temperature. Similarly, at the same shear rate, the viscosity of the composite gel samples decreases with increasing temperature. This can be attributed to the increase in internal energy and intensified molecular thermal and chain segment movements as the temperature rises. Consequently, the chemical bonds formed by the hydroxyl groups in the gelling agents (PVA, Gel, and CMC) and the borate ions in the cross-linking agents break, resulting in the inability to form an effective three-dimensional network structure. Additionally, the increase in the temperature accelerates the evaporation of water on the surface of the composite gel, leading to a reduction in its apparent viscosity. Zero shear viscosity, which is the limit value at which viscosity tends to zero with shear

https://doi.org/10.1021/acsomega.4c01502
ACS Omega 2024, 9, 28253−28267

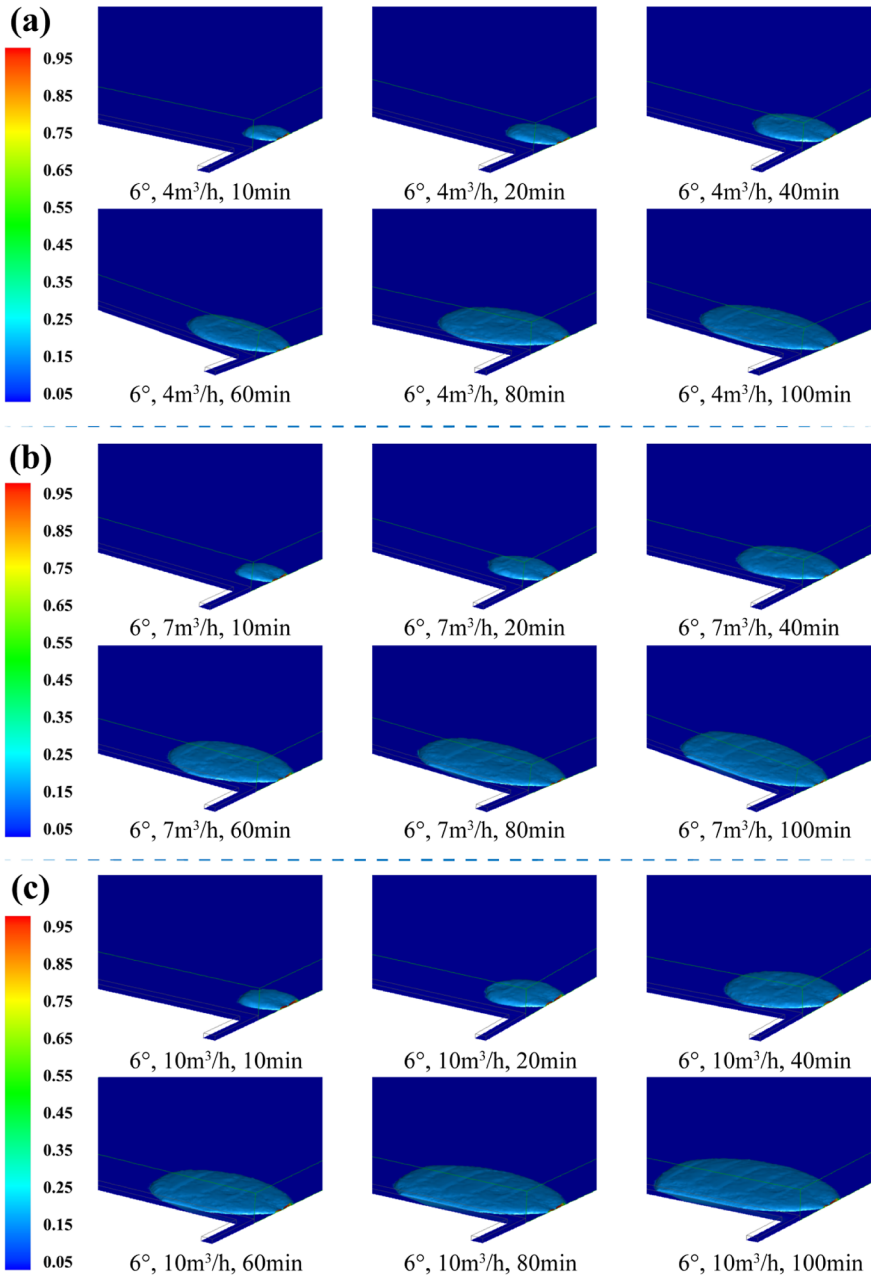

Figure 13. Seepage diffusion state of the composite gel when the dip angle of goaf is 6°: (a) 4; (b) 7; and (c) 10 m^3/h.

rate, is an important parameter for characterizing the rheological properties of polymers.[22] To calculate the zero shear viscosity of the gel, the logarithmic form of the Spencer–Dillon empirical formula (equation 2) is utilized.

$$\ln \eta = \ln \eta_0 - \frac{\tau}{b} \tag{2}$$

In the equation, η represents the apparent viscosity in m·Pa·s, η_0 represents the zero shear viscosity in m·Pa·s, and τ represents the shear stress in m·Pa. The parameter b represents the sensitivity of apparent viscosity to shear stress, and a smaller value of b indicates a greater sensitivity of η to τ.

To calculate the logarithm of the apparent viscosity of the sample in Figure 6 using eq 4, regression analysis was performed, and the results are presented in Figure 7 and Table 7.

From Figure 7 and Table 7, it can be seen that the ln of all data $\eta-\tau$ and the fitting degree are relatively high, with R^2 above 0.81. Furthermore, it is incorporated into the Arrhenius equation (equation 3)[23] to obtain the relationship between apparent viscosity and temperature.

$$\ln \eta = \ln A - \frac{E_a}{RT} \tag{3}$$

Among them, A represents the prefactor, m·Pa·s; R represents the molar gas constant, 8.314 J/(mol·K); T represents the thermodynamic temperature, K; and E_a represents the activation energy, J/mol.

Based on the data presented in Figure 8 and Table 8, it is evident that the curve adheres to the Arrhenius equation model with an R^2 value exceeding 0.96. As the temperature rises, the activation energy (E_a) also increases continuously, indicating a significant influence of temperature on the

https://doi.org/10.1021/acsomega.4c01502
ACS Omega 2024, 9, 28253−28267

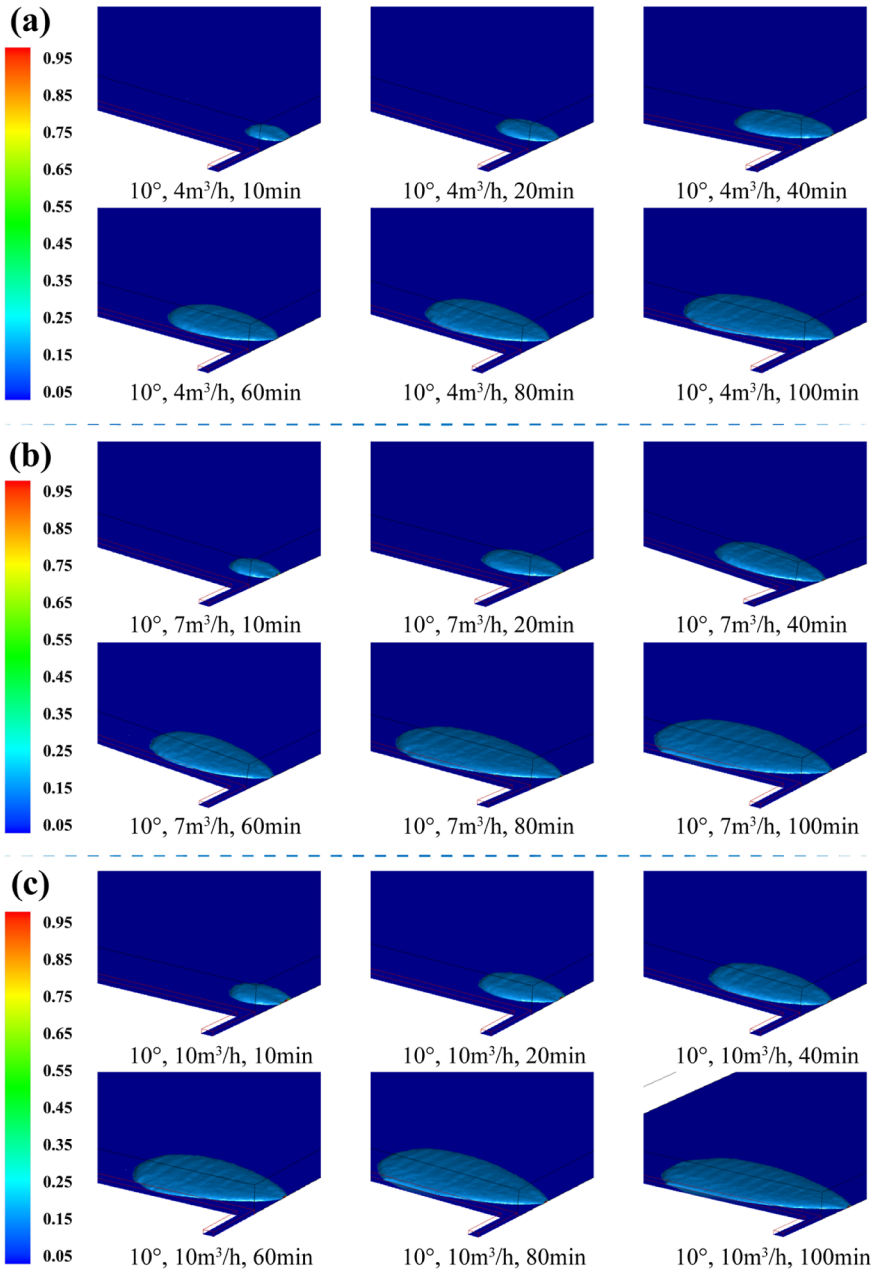

Figure 14. Seepage diffusion state of the composite gel when the dip angle of goaf is 10°: (a) 4; (b) 7; and (c) 10 m^3/h.

rheological behavior of the composite gel. The elevated temperature induces a greater flow energy resulting from changes in the molecular structure within the system. This, in turn, reduces the entanglement between molecular chains and prevents the formation of an effective three-dimensional network structure, ultimately leading to a decrease in the viscosity of the composite gel.

3.4. Rheological Properties of the Composite Gel under Different Shear Speeds. The apparent viscosity of samples at different rotational speeds (6, 12, 30, and 60 rpm) was determined at room temperature (30 °C). The mass concentration of the foaming agent (0.5% SDS:0.1% APG), calcium carbide slag mass (3.09 g), alcohol amine solution mass (7.5 g), and the amount of gelling agent added (30 g) were fixed, along with the same mass concentration of CO_2 gas. The rheological properties of the samples were analyzed to investigate the effects of different rotational speeds, as shown in Figure 9.

The results presented in Figure 9 demonstrate that the apparent viscosity of the composite gel remains relatively constant over time at a specific temperature, indicating excellent stability. The good stability of the composite gel can be attributed to the following mechanism: when the polymer is dissolved in water, the molecular chains adopt a fully stretched state due to the dissolution process. Under shear stress, the molecular chains align, and the entangled nodes decrease, leading to the disruption of the equilibrium three-dimensional network structure and a reduction in apparent viscosity. However, after a period of shearing, the directional arrangement of the molecular chains becomes relatively stable, resulting in a stabilized apparent viscosity of the composite gel.

https://doi.org/10.1021/acsomega.4c01502
ACS Omega 2024, 9, 28253−28267

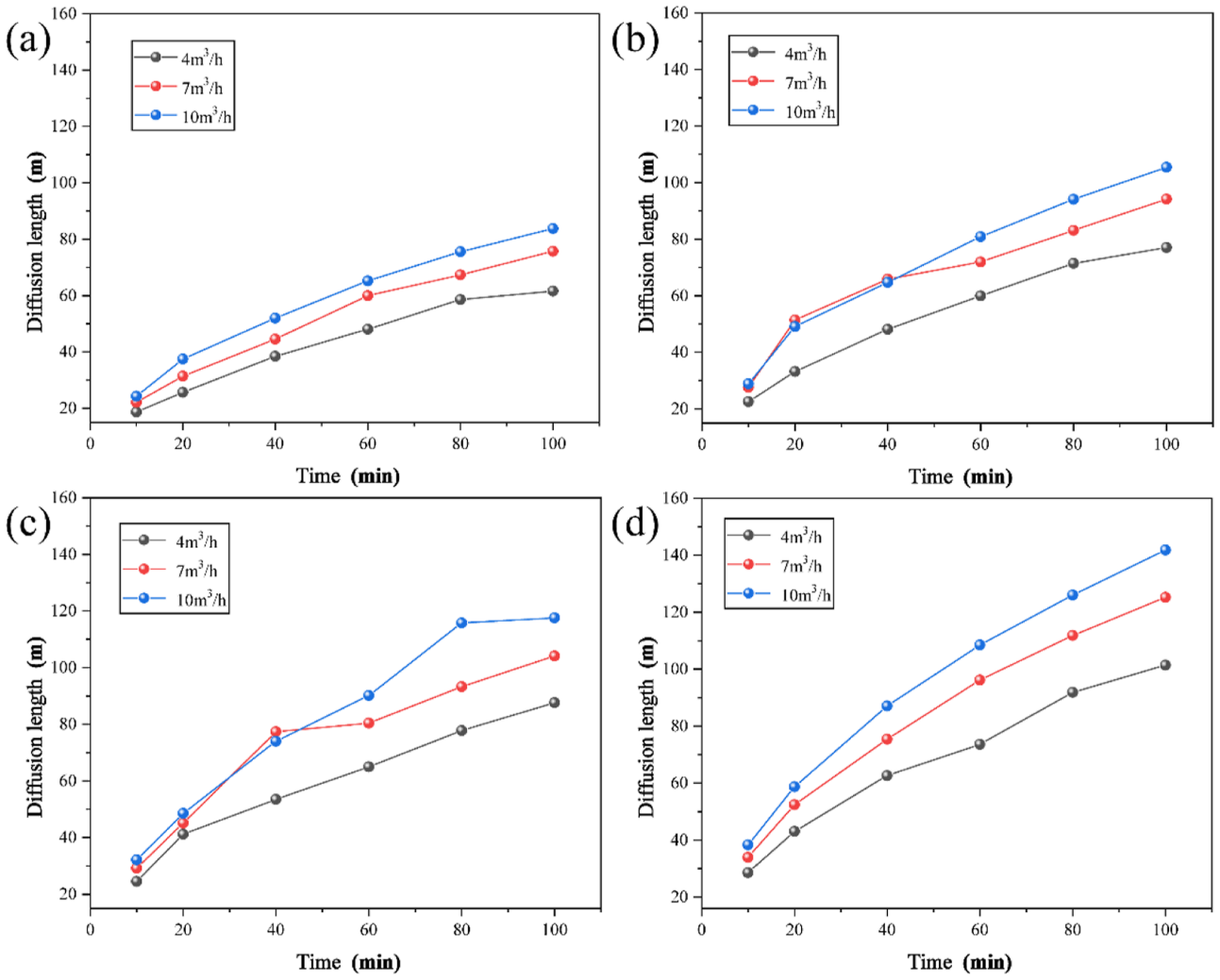

Figure 15. Diffusion length of the composite gel at different dip angles: (a) 2°; (b) 4°; (c) 6°; and (d) 10°.

The viscosity of the composite gel decreases as the shear rate increases. The flow behavior follows a typical pseudoplastic model, and its constitutive equation adheres to Ostwald's non-Newtonian fluid model.[24] Additionally, the apparent viscosity of the composite gel with respect to shear rate was further tested, and the relationship between shear stress and shear rate was obtained by binomial fitting the curve (Figure 10). The rheological equation of the composite gel is presented in Formula 4.

$$\tau = 76423 + 5417 \times \gamma - 55 \times \gamma^2 R^2 = 0.999 \quad (4)$$

when γ equal to 0, τ 76 423 m·Pa; when the shear stress is less than 76 423 m·Pa, the composite gel shows solid properties; on the contrary, it shows that the composite gel has the characteristics of fluidity.

3.5. Study on Seepage Diffusion Characteristics of the Composite Gel in Goaf. *3.5.1. Construction of a Mathematical Model of the Composite Gel in Goaf.* The goaf is filled with broken rock blocks and scattered coal bodies, with cracks spreading throughout the entire space. These characteristics align with the definition of porous media.[25] The seepage and diffusion of composite gel in the goaf's porous medium are influenced by various factors. To enhance the reliability of the established mathematical model, the following assumptions are made regarding the properties of the composite gel. ① The seepage of the composite gel in the goaf belongs to laminar flow and moves in an overall manner, which meets the continuous medium theory, and it is considered that gas compression has no effect on the seepage of the composite gel in the goaf. ② The composite gel does not have the fluid−solid coupling effect with rock and coal when it percolates in the goaf. ③ The permeability of the goaf is not related to the composite gel injection time but only to the depth of the goaf, that is, the distance from the working face. ④ The seepage process of the composite gel in the goaf conforms to the Darcy law modified by HB.

The flow of the composite gel in porous media adheres to the principles of conservation of mass, energy, and momentum. The control equation serves as the mathematical representation of these conservation laws. The mathematical model of compound gel flow in goaf is established by combining the control equation with specific boundary conditions and initial conditions.

According to the research in Section 3.5, the relationship between the shear stress and the shear rate of the composite gel is shown in formula 5

$$\tau = 76423 + 5417\gamma - 55\gamma^2 \quad (5)$$

Therefore, the apparent viscosity of the composite gel can be described by formula 6

https://doi.org/10.1021/acsomega.4c01502
ACS Omega 2024, 9, 28253−28267

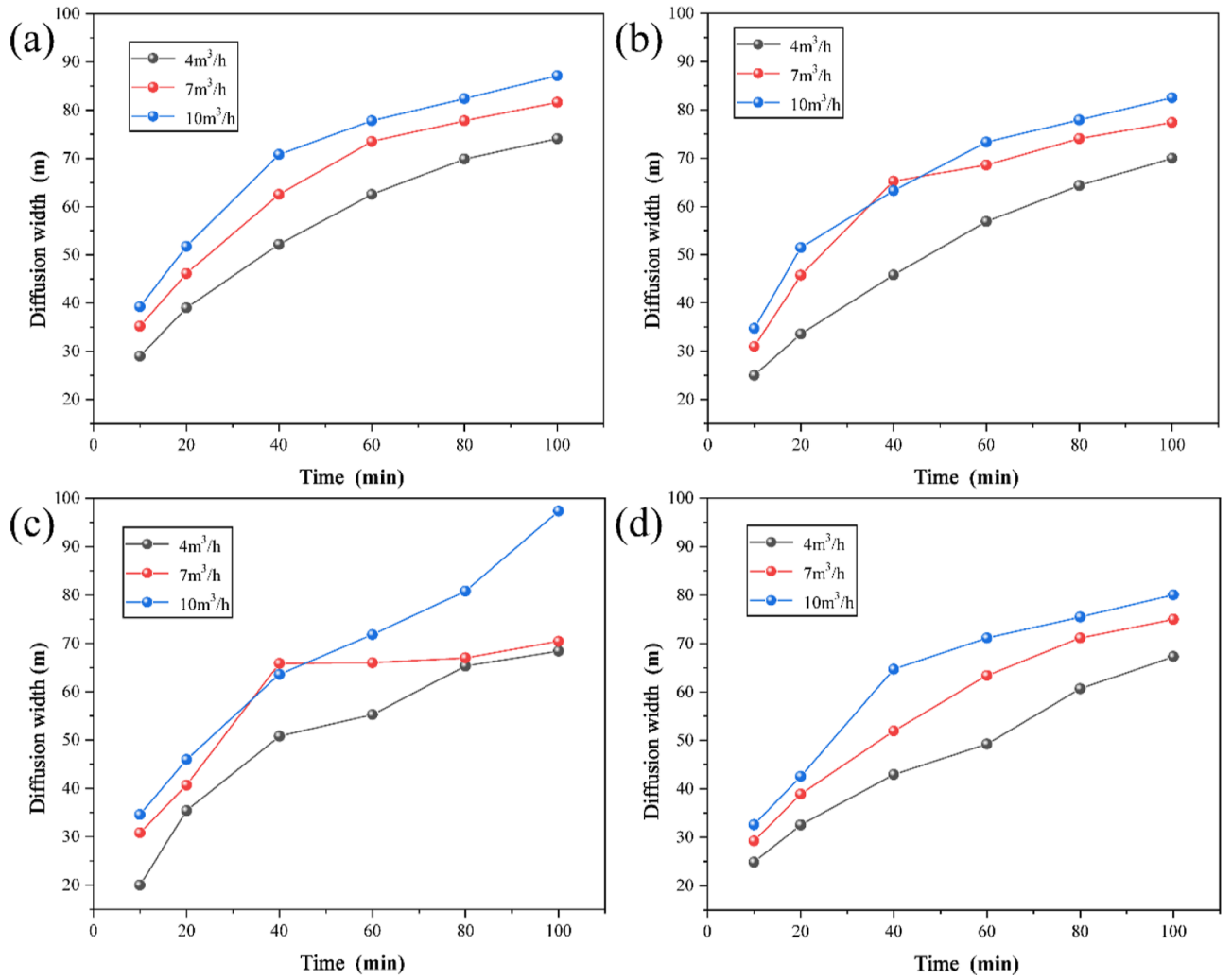

Figure 16. Diffusion width of the composite gel at different dip angles: (a) 2°; (b) 4°; (c) 6°; and (d) 10°.

Table 9. Annual Cost Analysis of the Porous Gel

materials	annual cost analysis
porous gel	amount of glue used: 10 t, frequency of use: 1 times/month, and annual amount of glue used: 12 × 1 × 10 t = 120 t
	the price of each component in porous gel: SDS: ¥7000/t, APG: ¥8000/t, PVA: ¥9000/t, Gel: ¥15 000/t, CMC: ¥4500/t, sodium tetraborate: ¥3500/t, TETA: ¥6000/t, carbide slag: ¥180/t, and water: ¥3/t
	per ton of porous gel: SDS: 1 t × 0.005 × ¥7000/t = ¥35, APG: 1 t × 0.001 × ¥8000/t = ¥8, PVA: 1 t × 0.04 × ¥9000/t = ¥360, gel: 1 t × 0.00025 × ¥15 000/t = ¥3.75, CMC: 1 t × 0.00025 × ¥4500/t = ¥1.125, sodium tetraborate: 1 t × 0.04 × ¥3500/t = ¥140; and TETA: 1 t × 0.075 × ¥6000/t = ¥450
	carbide slag: 1 t × 0.0309 × ¥180/t = ¥5.562, water: 1 t × 0.51 × ¥3/t = ¥1.53
	porous gel price per ton
	35 + 8 + 360 + 3.75 + 1.125 + 140 + 450 + 5.562 + 1.53 = ¥1004.967
	annual total price of porous gel required: ¥1004.967/t × 120 t = ¥120 596.04
	processing cost: about ¥60/t
	annual processing cost: 120 t × ¥60/t = ¥7200
	labor, equipment amortization, taxes, and administrative costs: ¥30/t
	annual labor, equipment amortization, taxes, and administrative costs
	120 t × ¥30/t = ¥3600
	total annual use cost: 120 596.04 + 7200 + 3600 = ¥131 396.04

$$\eta = 5417 + \frac{76423}{\gamma} - 55\gamma \quad (6)$$

At 30 °C, a composite gel sample with gelling agent [PVA/(Gel + CMC) = 20:10] of 30 wt %, cross-linking agent of 4 wt %, carbide slag of 3.09 wt %, alcohol amine solution of 7.5 wt %, and foaming agent of 0.5% SDS + 0.1% APG is prepared. Assuming that the composite gel can foam 20 times, the density of the composite gel is 60 kg/m^3.

3.5.2. Seepage Diffusion Characteristics of the Composite Gel under Different Conditions. In order to guide the

https://doi.org/10.1021/acsomega.4c01502
ACS Omega 2024, 9, 28253−28267

construction of a working face in a coal mine in Shaanxi Province, this study conducted numerical simulations on the seepage diffusion of the composite gel in the goaf. The dip angles of the working face were set to 2, 4, 6, and 10°, while the inlet velocities were set to 4, 7, and 10 m^3/h. For clarity, this study defines the diffusion length of the composite gel as the direction along the goaf dip with the pouring mouth as the boundary. The diffusion front edge refers to the direction along the pouring speed, while the diffusion rear edge refers to the direction opposite the pouring direction. The sum of the diffusion front edge and the diffusion rear edge is defined as the diffusion width of the composite gel.

Figures 11−14 illustrate the seepage diffusion state of a composite gel in the goaf under different dip angles and inlet velocities. The diffusion profile of the composite gel in the figure represents a coverage rate of 20%. From Figure 11, it can be observed that at a dip angle of 2°, with fixed injection inlet velocities of 4, 7, and 10 m^3/h, the diffusion area of the composite gel gradually increases as the injection time extends from 10 to 100 min. The diffusion width of the composite gel along the direction of the goaf aligns with the diffusion length along the working face trend. The diffusion area of the fixed composite gel gradually increases with the increase of injection inlet speed (4, 7, and 10 m^3/h), indicating that both the injection inlet speed and injection time have a similar effect on the diffusion area of the composite gel in the goaf. When the dip angle of the goaf is 4° (as shown in Figure 12), the trend of the diffusion area of the composite gel in the goaf is similar to that at a dip angle of 2°. Its diffusion area increases with time migration and with the increase of the injection inlet speed. However, the length of the dip along the working face is greater than the diffusion width along the direction of the goaf. After 40 min of diffusion time, the morphology of the diffusion area is approximately "oval". This may be attributed to the presence of a gravity component along the direction of the working face in the composite gel. As the dip angle of the goaf continues to increase (as shown in Figures 13 and 14), the diffusion area of the composite gel increases with the increase of the injection inlet speed and time. Furthermore, the diffusion length along the dip direction of the working face is significantly greater than the diffusion width along the strike of the goaf.

According to Figures 11−14, it can be observed that during the initial stage (0−40 min) of diffusion in the goaf, both the diffusion length and width of the composite gel increase rapidly. However, during the later stage (60−100 min) of diffusion, the diffusion distance of the composite gel increases at a slower rate. In the following section, a detailed analysis of the diffusion length and width of the composite gel in the goaf will be presented.

3.5.3. Diffusion Distance of the Composite Gel under Different Conditions. Figures 15 and 16 display the diffusion length and width of the composite gel in the goaf under different goaf dip angles and injection inlet velocities. In Figures 15a and 16a, it is observed that when the goaf dip angle is 2° and the injection inlet velocities are 4, 7, and 10 m^3/h, the diffusion lengths of the composite gel within the first 10 min are 18.72, 22.11, and 24.26 m, respectively. Similarly, the diffusion widths are 28.99, 35.20, and 39.26 m, respectively. After 100 min, the diffusion length of the composite gel reaches 65.19, 75.71, and 83.74 m, while the diffusion width reaches 74.07, 81.63, and 87.15 m, respectively. Notably, the diffusion width of the composite gel in the goaf consistently exceeds the diffusion length, indicating that the diffusion distance is longer in the direction of the goaf trend, irrespective of the injection speed.

The results shown in Figures 15b and 16b indicate that for a dip angle of 4° and injection inlet velocities of 4, 7, and 10 m^3/h, the diffusion lengths of the composite gel in the first 10 min are 22.59, 27.60, and 28.90 m, respectively. Similarly, the diffusion widths are 25.00, 30.96, and 34.72 m. After 100 min, the diffusion lengths of the composite gel are 77.00, 94.20, and 105.40 m, while the diffusion widths are 70.00, 77.40, and 82.50 m. At the initial stage of perfusion, the diffusion width is greater than the diffusion length at this inclination angle. However, as the perfusion time increases, the diffusion length gradually exceeds the diffusion width. This transition in diffusion distance occurs within 20−40 min of perfusion. The reason for this change is that although the dip angle of the goaf produces a gravity component that acts on the composite gel, it is not as strong as the driving force generated by the injection inlet along the direction of the goaf. Therefore, when the dip angle is 2°, the diffusion width of the composite gel is always greater than the length. As the dip angle increases, the driving force along the dip direction also increases, resulting in a longer diffusion distance along that direction under these boundary conditions.

Figures 15c and 16c demonstrate that when the dip angle of the goaf is 6°, the composite gel's diffusion length at the end of perfusion is 87.60, 104.10, and 117.60 m, while the width is 68.40, 70.40, and 97.35 m, respectively. It is observed that at this dip angle, the driving force generated by the dip angle surpasses that generated by the injection inlet velocity. Furthermore, the diffusion distance of the composite gel in the goaf along the dip direction is significantly greater than that along the trend direction. On the other hand, when the dip angle of the gob is 10° (Figures 15d and 16d), the composite gel continues to increase along the dip direction of the gob. At the end of grouting, the diffusion length reaches 101.42, 125.20, and 141.85 m, respectively, but decreases along the direction of the gob. At the end of grouting, the diffusion width is only 67.29, 75.00, and 80.06 m, respectively.

Based on the analysis above, it is evident that both the diffusion length and width of the composite gel increase gradually as the perfusion inlet velocity increases. Furthermore, as the dip angle of the goaf increases, the diffusion length increases gradually, while the diffusion width decreases gradually. It is worth noting that although there is an abnormal diffusion width observed when the dip angle of the goaf is 6° and the injection inlet speed is 10 m^3/h, it does not significantly impact the overall diffusion trend of the composite gel in the goaf.

3.6. Economic Benefit Analysis. China's production of bulk industrial solid waste is large. In 2021, China's national output of general industrial solid waste was 3.97 billion tons. In this study, calcium-based solid waste (calcium carbide slag) and triethylenetetramine were used to mineralize CO_2, which realized the maximum utilization of resources and provided a new way to solve the utilization problem of calcium carbide slag. Considering the field application, it is assumed that the amount of glue used per year is 120 t, and the cost of using porous gel is calculated, as shown in Table 9. As can be seen from the table, the annual cost of porous gel raw materials is 120 596.04 ¥, and the total annual use cost is ¥131 396.04. The costs of mineralizing a ton of CO_2 at different temperatures were about ¥15 642.39 (20 °C), ¥14 220.35 (30 °C), and

https://doi.org/10.1021/acsomega.4c01502
ACS Omega 2024, 9, 28253−28267

¥9954.25 (40 °C), respectively. The popularization and use of porous gel materials is conducive to absorbing bulk industrial solid waste and reducing the total carbon emissions of greenhouse gases. It is beneficial to protect natural resources, reduce energy consumption, and meet the requirements of low-carbon economy.

4. CONCLUSIONS

The ratio, influencing factors, and rheological properties of the composite gel were systematically studied through a single-factor test. The following conclusions were drawn.

(1) The study examined the effects of the proportion of PVA in the gelling agent and the amount of cross-linking agent on the apparent viscosity of the composite gel. The rheological curves of the composite gel showed a "hysteresis loop", indicating the presence of thixotropy in the composite gel system.

(2) The constitutive equation of the composite gel adheres to the Ostwald non-Newtonian fluid equation. The curves of the composite gel system exhibit a linear function relationship, with a power law index less than 1. The rheological function of the composite gel is as follows: $\tau = -55\gamma^2 + 5417\gamma + 76\,423$. When the shear rate is 0, the shear stress (τ) is 76 423 m·Pa. When the shear stress is less than 76 423 mPa, the system exhibits a solid morphology, while when the shear stress is greater than 76 423 mPa, the system exhibits a fluid morphology.

(3) The seepage diffusion characteristics of the composite gel in the goaf were investigated through numerical simulation. The results indicate that the dip angle of the goaf and the injection inlet velocity significantly influence the diffusion of the composite gel. The diffusion distance increases with higher injection inlet velocity and a steeper dip angle of the goaf.

AUTHOR INFORMATION

Corresponding Author

Qian Zhang − *Key Lab of Mine Disaster Prevention and Control, School of Safety and Environmental Engineering, Shandong University of Science and Technology, Qingdao, Shandong 266590, China*; orcid.org/0000-0002-5562-860X; Email: 528243891@qq.com

Authors

Xiaonan Shi − *School of Statistics and Data Science, Qufu Normal University, Qufu, Shandong 273165, China*

Baiqian Wu − *Key Lab of Mine Disaster Prevention and Control, School of Safety and Environmental Engineering, Shandong University of Science and Technology, Qingdao, Shandong 266590, China*

Xuechao Dong − *Key Lab of Mine Disaster Prevention and Control, School of Safety and Environmental Engineering, Shandong University of Science and Technology, Qingdao, Shandong 266590, China*

Wei Lu − *School of Energy and Safety Engineering, Anhui University of Science and Technology, Huainan, Anhui 232001, China*

Xiaolin Chen − *School of Statistics and Data Science, Qufu Normal University, Qufu, Shandong 273165, China*

Complete contact information is available at: https://pubs.acs.org/10.1021/acsomega.4c01502

Notes

The authors declare no competing financial interest.

ACKNOWLEDGMENTS

We are grateful for joint funding by the National Natural Science Foundation of China (no. 51974178 and no. 42307585), Class A Talent Project of Shandong University of Science and Technology Elite Program (22-003; 22-013), Qingdao Natural Science Foundation (no. 2321101-zyyd-jch), and Shandong Natural Science Foundation (no. ZR2023QE042 and no. ZR2023QE013).

REFERENCES

(1) Qiao, J.; Zhao, D.; Zhao, Y. Y.; Lu, W.; Li, M. M.; Hu, X. M.; Liang, Y. T.; Tian, F. C.; Ju, S.; Yan., B. R. Preparation and characteristics of sustained-release microcapsule-based inhibitory foam with high foaming ratio. *Fuel* **2021**, *302*, 121219.

(2) Li, Y. S.; Hu, X. M.; Cheng, W. M.; Shao, Z.; Xue, D.; Zhao, Y. Y.; Lu, W. A novel high-toughness, organic/inorganic double-network fire-retardant gel for coal-seam with high ground temperature. *Fuel* **2020**, *263*, 116779.

(3) Fan, Y. J.; Zhao, Y. Y.; Hu, X. M.; Wu, M. Y.; Xue, D. A novel fire prevention and control plastogel to inhibit spontaneous combustion of coal: Its characteristics and engineering applications. *Fuel* **2020**, *263*, 116693.

(4) Hu, X. M.; Cheng, W. M.; Nie, W.; Wang, D. M. Flame Retardant, Thermal, and Mechanical Properties of Glass Fiber/Nanoclay Reinforced Phenol-Urea-Formaldehyde Foam. *Polym. Composit.* **2016**, *37*, 2323−2332.

(5) Lu, W.; Hu, H.; Qi, G. S. Effect of Pipe Diameter and Inlet Parameters on Liquid CO_2 Flow in Transportation by Pipeline with Large Height Difference. *Processes* **2019**, *7*, 756.

(6) Cheng, W. M.; Hu, X. M.; Xie, J.; Zhao, Y. Y. An intelligent gel designed to control the spontaneous combustion of coal: Fire prevention and extinguishing properties. *Fuel* **2017**, *210*, 826−835.

(7) Qin, B. T.; Lu, Y.; Li, Y.; Wang, D. M. Aqueous three-phase foam supported by fly ash for coal spontaneous combustion prevention and control. *Adv. Powder Technol.* **2014**, *25*, 1527−1533.

(8) Shi, Q. L.; Qin, B. T.; Hao, Y. H.; Li, H. B. Experimental investigation of the flow and extinguishment characteristics of gel-stabilized foam used to control coal fire. *Energy* **2022**, *247*, 123484.

(9) Liu, X. Y.; Cheng, H.; Lin, J.; Rong, C. X.; Li, M. J.; Xu, H. D. Study of the Mechanism of Fracture Grouting in Deeply Buried Rock Strata Based on Bingham Fluid Slurry. *Adv. Civ. Eng.* **2019**, *2019*, 1−10.

(10) Niu, J. D.; Li, Z. W.; Gu, W. H.; Chen, K. Experimental Study of Split Grouting Reinforcement Mechanism in Filling Medium and Effect Evaluation. *Sensors* **2020**, *20*, 3088.

(11) Feng, X.; Zhang, Q. S.; Jiang, Q. C.; Song, S. G.; Kong, X. H.; Liu, R. T.; Xie, C. Study on variation law of cement slurry density in porous media considering convection-diffusion-infiltration. *Arab. J. Geosci.* **2019**, *12*, 742.

(12) Li, S. C.; Pan, D. D.; Xu, Z. H.; Lin, P.; Zhang, Y. C. Numerical simulation of dynamic water grouting using quick-setting slurry in rock fracture: the Sequential Diffusion and Solidification (SDS) method. *Comput. Geotech.* **2020**, *122*, 103497.

(13) Zhang, E.; Xu, Y. C.; Fei, Y.; Shen, X. Y.; Zhao, L.; Huang, L. Influence of the dominant fracture and slurry viscosity on the slurry diffusion law in fractured aquifers. *Int. J. Rock. Mech. Min.* **2021**, *141*, 104731.

(14) Liang, J. S.; Ma, S. K.; Du, X. M. Diffusion Model of Parallel Plate Crack Grouting Based on Foaming Expansion Characteristics of Polymer Slurry. *Mathematics* **2021**, *9*, 2907.

(15) Yang, Z. Q.; Chen, M.; Ding, Y.; Yang, Y.; Zhu, Y. Y.; Guo, Y. H.; Wang, R. C.; Zhang, B. H.; Fang, Y. C.; Yu, D. L.; et al. Influence of Coupling Effects of Time and Water-to-Cement Ratio on Rheological Properties of Bingham Cement Grouts. *Adv. Mater. Sci. Eng.* **2021**, *2021*, 1−10.

(16) Mauludin, L. M.; Zhuang, X. Y.; Rabczuk, T. Computational modeling of fracture in encapsulation-based self-healing concrete using cohesive elements. *Compos. Struct.* **2018**, *196*, 63−75.
(17) Böhme, G. Non-Newtonian fluid mechanics. Lecture. **1987**, *15*, 241−260.
(18) Hong, F. U.; Wei, Y.; Ding, Y.; Zhu, J.; Bioengineering, D. O. Infinitesimal method and its application in deriving the measurement principle of Ostwald viscometer. *Chin. J. Med. Phys.* **2017**, *34*, 848−849.
(19) Musa, A. Y.; Kadhum, A. A. H.; Mohamad, A. B.; Rahoma, A. A. B.; Mesmari, H. Electrochemical and quantum chemical calculations on 4,4-dimethyloxazolidine-2-thione as inhibitor for mild steel corrosion in hydrochloric acid. *J. Mol. Struct.* **2010**, *969*, 233−237.
(20) Finšgar, M.; Lesar, A.; Kokalj, A.; Milošev, I. A comparative electrochemical and quantum chemical calculation study of BTAH and BTAOH as copper corrosion inhibitors in near neutral chloride solution. *Electrochim. Acta* **2008**, *53*, 8287−8297.
(21) Abbasi, F. M.; Shehzad, S. A. Heat transfer analysis for three-dimensional flow of Maxwell fluid with temperature dependent thermal conductivity: Application of Cattaneo-Christov heat flux model. *J. Mol. Struct.* **2016**, *220*, 848−854.
(22) Li, G. N.; Tan, Y. Q.; Fu, Y. K.; Liu, P. F.; Fu, C. L.; Oeser, M. Density, zero shear viscosity and microstructure analysis of asphalt binder using molecular dynamics simulation. *Constr. Build. Mater.* **2022**, *345*, 128332.
(23) Bhatti, M. M.; Michaelides, E. E. Study of Arrhenius activation energy on the thermo-bioconvection nanofluid flow over a Riga plate. *J. Therm. Anal. Calorim.* **2021**, *143*, 2029−2038.
(24) Martyushev, L. M.; Birzina, A. Morphological stability of an interface between two non-Newtonian fluids moving in a Hele-Shaw cell. *Phys. Rev. E: Stat., Nonlinear, Soft Matter Phys.* **2015**, *91*, 013004.
(25) Wang, G.; Xu, H.; Wu, M. M.; Wang, Y.; Wang, R.; Zhang, X. Q. Porosity model and air leakage flow field simulation of goaf based on DEM-CFD. *Arab. J. Geosci.* **2018**, *11*, 148.

https://doi.org/10.1021/acsomega.4c01502
ACS Omega 2024, 9, 28253−28267